Journal of Non-Crystalline Solids 358 (2012) 2910–2916

Contents lists available at SciVerse ScienceDirect

Journal of Non-Crystalline Solids

journal homepage: www.elsevier.com/ locate/ jnoncrysol

Synchrotron radiation photoelectron spectroscopy studies of self-organization in $As_{40}Se_{60}$ nanolayers stored under ambient conditions and after laser irradiation

O. Kondrat [a,*], N. Popovich [a], R. Holomb [a], V. Mitsa [a], V. Lyamayev [b], N. Tsud [c], V. Cháb [d], V. Matolín [c], K.C. Prince [b,e]

[a] Institute of Solid State Physics and Chemistry, Uzhhorod National University, Pidhirna str., 46, 88000 Uzhhorod, Ukraine
[b] Sincrotrone Trieste S.C.p.A., Strada Statale 14, km 163.5, 34149 Basovizza, Trieste, Italy
[c] Charles University, Faculty of Mathematics and Physics, Department of Surface and Plasma Science, V Holešovičkách 2, 18000 Prague 8, Czech Republic
[d] Institute of Physics, Academy of Sciences of the Czech Republic, Cukrovarnická 10, 16253 Prague 6, Czech Republic
[e] IOM-CNR, 34149 Basovizza, Trieste, Italy

ARTICLE INFO

Article history:
Received 5 June 2012
Received in revised form 17 July 2012
Available online 8 August 2012

Keywords:
Chalcogenide glass;
$As_{40}Se_{60}$;
Photostructural changes;
Photoelectron spectroscopy

ABSTRACT

The influence of air and near bandgap laser irradiation on the surface structure of $As_{40}Se_{60}$ nanolayers has been investigated by synchrotron radiation photoelectron spectroscopy (SRPES). The As 3d and Se 3d photoemission peaks of the irradiated sample show significant differences in shapes and positions in comparison with those obtained for non-irradiated amorphous films. The experimental data processing and quantification were performed by analyzing As 3d, Se 3d, C 1s and O 1s core-level components obtained by curve fitting. The relative contribution of the As, Se, C and O atoms in different chemical states to the whole As 3d, Se 3d, C 1s and O 1s signals, its structural origins as well as their relation to the $As_{40}Se_{60}$ surface and subsurface nanolayers structure before and after laser irradiation is analyzed and discussed in detail. An atomic model of induced structural changes on the surface of $As_{40}Se_{60}$ nanolayers under ambient conditions and after laser irradiation in air is proposed.

1. Introduction

Chalcogenide glassy (ChG) materials discovered by N.A. Gorynova and B.T. Kolomiyets in mid 1950s [1] have a special place among semiconductors because their fundamental study formed the basis for a general understanding of electronic phenomena in disordered structures [2,3]. Amorphous chalcogenides have been of great interest due to their remarkable structural, electronic and optical properties and have a wide range of potential applications [4]. Many properties of chalcogenide glasses show sensitivity to near band-gap light. The photons may affect electrical, chemical, optical, volume or mechanical properties of glasses [5,6]. These changes can be transient, metastable or permanent. On the bases of these phenomena (*i.e.* light sensitive properties of chalcogenide glasses and especially their amorphous thin films) numerous applications have been devised [7,8].

In general, the photoinduced effects are believed to arise from the excitation of electrons across the bandgap (*e.g.* photodarkening [9,10]) and consequent atomic displacements (*e.g.* in photocrystallization [11], photoexpansion [12], and opto-mechanical effects [8]). Recent studies on photoinduced effects such as photoexpansion of chalcogenide films suggest a uniform expansion of the material from photorelaxation, but other investigations indicate photoinduced oxidation as a main effect [13–15]. Therefore, it is important to understand the role of the ambient conditions in the observed photoinduced phenomena.

Numerous experimental techniques have been used to investigate and characterize the structure of non-crystalline chalcogenides at the nanoscale, including conventional diffraction methods, inelastic neutron and Raman scattering [16]. Structural modeling, *i.e.* molecular dynamics (MD) simulations and *ab initio* calculations have also been applied to the interpretation of the experimental results [17]. For nonlinear optical devices based on ChGs the propagation loss of the waveguide is a significant factor determining performance [18]. Absorption from homopolar and dangling bonds, and surface oxidization lead to higher light attenuation in films [18,19].

In this paper we report results on the investigation of light-induced structural changes of amorphous $As_{40}Se_{60}$ thin films at the atomic scale (i), determination of the influence of air exposure on surface structure (ii), and finally comparison the types and concentrations of different structural units (s.u.) in the $As_{40}Se_{60}$ film before and after laser irradiation (iii) by means of SRPES.

2. Experimental details

The bulk $As_{40}Se_{60}$ samples were prepared by the conventional melt-quenching route in evacuated quartz ampoules from a mixture of high purity 99.999% As and Se precursors. The furnace was rocked to obtain the most homogeneous melt. All ingots were quenched by switching off the furnace. Amorphous $As_{40}Se_{60}$ thin films with thickness of about

* Corresponding author. Tel.: +38 031 22 33020; fax: +38 031 22 32339.
E-mail address: kon_alex@gala.net (O. Kondrat).

0022-3093/$ – see front matter © 2012 Elsevier B.V. All rights reserved.
http://dx.doi.org/10.1016/j.jnoncrysol.2012.07.025

500 Å were prepared by thermal evaporation of bulk glass onto (100) silicon crystal wafer substrates. For the laser irradiation experiment, the amorphous $As_{40}Se_{60}$ thin film was covered by aluminum foil with a hole of ~3 mm diameter. The irradiation was carried out in air at room temperature for ~3 h by a He–Ne (632.8 nm) laser of 50 mW/cm^2 intensity. The laser intensity and exposure were chosen based on our previous studies of As–Se glasses by means of Raman spectroscopy.

Photoemission measurements were performed at the Materials Science Beamline of the Elettra Synchrotron light source (Trieste, Italy). The surfaces of the films were cleaned by Ar-ion sputtering. To minimize possible changes of surface As/Se stoichiometry due to Ar-ion bombardment, low sputtering exposure (500 V, 5 min) was used, enough for removal of only the top impurity overlayer. The photoemission spectra were taken using synchrotron light with photon energy of 450 eV for As 3d, Se 3d, C 1s core levels and 600 eV for O 1s core level at normal emission geometry. Photoemission spectra were recorded using the PHOIBOS 150 multi-channel hemispherical analyzer, with a step of 0.05 eV and pass energy of 10 eV. The SRPES peak intensities were measured with accuracy better than ~5% and were normalized to the incident photon flux. The As 3d, Se 3d, C 1s and O 1s core-level spectra of as-prepared and laser irradiated $As_{40}Se_{60}$ films were measured with total (photon beam + analyser + natural line width) energy resolution of 0.5 eV. Charging was observed for all samples. For the correction of this effect, the binding energy (BE) of a surface impurity C 1s signal (285.0 eV) was used which was crosschecked using the BE of the Se $3d_{5/2}$ bulk signal (54.7 eV) [20]. The charging potential was very slightly (~0.1 eV) different for films before and after irradiation, indicating a minor change in conductivity. For the amorphous and cleaned $As_{50}Se_{50}$ film we did not observe the usual signs of significant charging, which are shoulders on the high BE side of Se 3d core level spectra and broadening of the core level peaks. The same is true for the measured As 3d core level of irradiated $As_{40}Se_{60}$ film. Also, we checked the evolution of Se 3d and As 3d core level spectra under X-rays during the time necessary for recording the spectra and we found that the position and shape of the spectral features are stable with time. To accommodate differences in surface potentials between samples, and to determine the absolute positions of all SRPES core levels, an ultrathin (~3 Å) gold film was deposited on the sample surface just before the measurements. Then the experimental positions of the core levels for all the investigated samples were calibrated by referencing to the $4f_{7/2}$ core level peak of pure Au at 84.0 eV [21]. The gold-deposited sample was used only for the determination of absolute position and for controlling the studied core level shapes. The measured intensities of synchrotron radiation excited As 3d, Se 3d, O 1s, and C 1s core level spectra were normalized by the corresponding atomic photoionization cross-sections [22,23].

The Se 3d, As 3d, C 1s and O 1s core level peaks were fitted using a Voigt function with subtraction of a Shirley type background to yield peak position and intensity. The statistical branching ratio of 3:2 was used for the $3d_{5/2}$ and $3d_{3/2}$ spin-orbit split Se 3d and As 3d core level intensities. Doublet separations of 0.69 and 0.86 eV were used for As 3d and Se 3d core levels, respectively. The full-width-at-half-maximum (FWHM) was set to the same value for each doublet with the same origin while it was kept free for all individual components. The binding energy and the intensity of the $3d_{5/2}$ peaks of each doublet were allowed to vary freely and independently of each other. The standard errors of areas and BEs of fitted components were ±4% and ±0.05 eV respectively.

3. Results

3.1. Synchrotron radiation excited photoelectron spectra of $As_{40}Se_{60}$ amorphous non-irradiated and laser irradiated films

The Se 3d, As 3d, C 1s and O 1s core level spectra of amorphous non-irradiated (a) and irradiated (b) $As_{40}Se_{60}$ films together with the results of curve fitting are shown in Fig. 1. It is evident that the peak intensities and shapes are different for non-irradiated and irradiated samples while the BEs of peak components are nearly the same. Detailed analysis of the Se 3d core levels for the non-irradiated sample shows that the best fit is obtained when three components (spin-orbit split doublets) were used (Fig. 1, a). The BE of the main Se 3d component at ~54.7 eV (peak 1) is connected with the As—**Se**—As s.u. [20] and is characteristic of the As—**Se**—As s.u. in crystalline As_2Se_3. Two additional components observed in the Se 3d spectra of uncleaned sample were found at ~55.2 eV (peak 2) and ~55.6 eV (peak 3). According to published data [21], the first one can be assigned to Se-rich As—**Se**—Se or/and As—**Se**—C. The second component situated at 55.6 eV is due to the Se—**Se**—Se s.u. Therefore, the analysis of Se 3d spectra of amorphous $As_{40}Se_{60}$ films shows the presence of homopolar Se—Se bonds (As—**Se**—Se s.u.) and interface Se—C bonds at the surface. The increase of the Se 3d component BE up to 55.6 eV indicates that even chain-like Se motifs can be found in the structure of amorphous $As_{40}Se_{60}$ (Se—**Se**—Se coordination geometry).

To obtain a good fit of the As 3d spectra of the non-irradiated sample, two components were used (Fig. 1, a). These components were assigned to arsenic bonded to two selenium and one arsenic atoms (2Se—**As**—As, ~42.5 eV, peak2) and arsenic bonded to three selenium atoms (**As**—3Se, ~42.9 eV, peak 3) s.u. Their BEs are in good agreement with values reported for known materials with corresponding arsenic chemical coordination: As_4Se_4, and As_2Se_3, respectively [21,24–27]. Thus, two types of arsenic coordination may be resolved and used to explore the structure of $As_{40}Se_{60}$ nanolayers at the atomic scale.

Carbon and oxygen were detected in the surface region of amorphous non-irradiated chalcogenide $As_{40}Se_{60}$ nanolayers exposed to air under ambient condition. Fitting results of the measured C 1s core level spectra of amorphous $As_{40}Se_{60}$ films are shown in Fig. 1, a. As can be seen three components were used to obtain a good fit: C bonded to Se (at ~284.5 eV, peak 1), C bonded to C (at ~285.0 eV, so called graphitic peak, peak 2) and C bonded to O (at ~286.5 eV, peak 3). The presence of the **C**—Se peak is consistent with the presence of the corresponding component in Se 3d core level spectra and was also observed in Ref. [28]. The **C**—C and **C**—O component BEs are in accordance with published data [21].

The detailed analysis of the O 1s core level spectra revealed one component only which is located at ~532.0 eV and related to the presence of **O**—C bonds [29]. It correlates well with the corresponding **C**—O component (peak 3) found in the C 1s spectrum.

Similar spectra of laser irradiated $As_{40}Se_{60}$ films are shown in Fig. 1, b. The peak fitting was done using similar components as for the air-exposed sample. Simple comparison of Se 3d, As 3d, C 1s and O 1s core level spectra of amorphous (a) and irradiated (b) films shows that laser irradiation of $As_{40}Se_{60}$ film leads to changes of the peak shape and redistributions of the peak component intensities while the number of components in each peak and their positions are nearly the same. Peak 2 in Se 3d core level spectra became the most intensive and its energy position shifts to ~55.1 eV in comparison with the ~55.2 eV for the non-irradiated sample (Fig. 1). Peak 3 in the As 3d spectrum became more intense. A redistribution of intensity between peaks 1 and 2 in the C 1s spectrum is detected while no significant changes of the shape and position are detected for O 1s core level spectra.

3.2. Synchrotron radiation excited photoelectron spectra of Ar-ion cleaned $As_{40}Se_{60}$ amorphous non-irradiated and laser irradiated films

Additional measurements were performed on Ar-ion cleaned $As_{40}Se_{60}$ films before and after laser irradiation. Fig. 2 shows Se 3d, As 3d, C 1s and O 1s core level spectra of amorphous non-irradiated (a) and irradiated (b) Ar-ion cleaned $As_{40}Se_{60}$ films together with the results of curve fitting. In contrast to Fig. 1, the Se 3d core level of the non-irradiated Ar-ion cleaned sample is described by 2 components located at ~54.7 eV (peak 1) associated with the As—**Se**—As s.u., and at ~55.2 eV (peak 2) associated with the As—**Se**—Se and/or As—**Se**—C s.u. [20] (Fig. 2, a). Also an essential change was observed

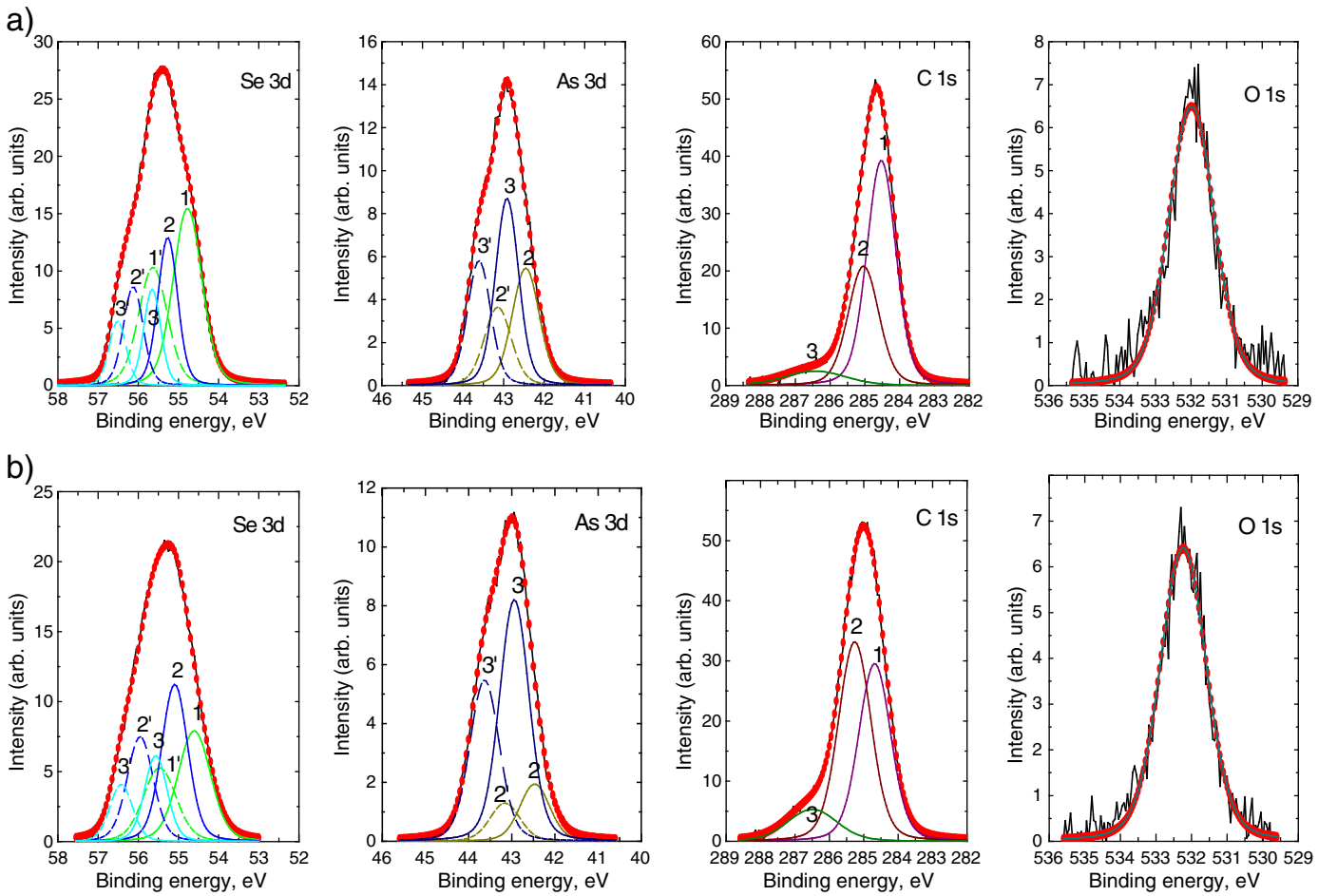

Fig. 1. Se 3d, As 3d, C 1s and O 1s core level spectra of amorphous non-irradiated (a) and irradiated (b) $As_{40}Se_{60}$ films (black solid line) together with the results of curve fitting (red dots). Se 3d peak components were identified as As—**Se**—As (1), As—**Se**—Se, As—**Se**—C (2), Se—**Se**—Se (3); for As 3d – 2Se—**As**—As (2), **As**—3Se (3); for C 1s – **C**—Se (1), **C**—C (2), **C**—O (3); for O 1s – **O**—C. Continuous and dotted lines denote $3d_{5/2}$ and $3d_{3/2}$ peaks, respectively. Photon energies: 450 eV for Se 3d, As 3d and C 1s; 600 eV for O 1s core levels.

in the As 3d core level spectra of the non-irradiated Ar-ion cleaned samples in comparison with the uncleaned one, and three components were obtained by fitting the As 3d spectra. The structural origin of two of them, peaks 2 and 3, is identical with the corresponding peaks detected for the uncleaned sample. We assign the additional peak at ~42.1 eV (peak 1) to As in As-rich 2As—**As**—Se s.u. (arsenic bonded to one selenium and two arsenic atoms). The C 1s signal from the cleaned sample was very weak and only one peak (at ~284.5 eV, peak 1, **C**—Se bond) is resolved, and only a negligible oxygen contribution was detected.

A significant increase in peak intensity of the As—**Se**—Se or/and As—**Se**—C s.u. (peak 2) was observed in the Se 3d core level of the irradiated and cleaned $As_{40}Se_{60}$ film in comparison with the non-irradiated cleaned sample (Fig. 2, b). Also, a small change in BE of this peak is observed. In As 3d core level spectra of the irradiated and cleaned $As_{40}Se_{60}$ film, peak 1 disappears and peak 3 becomes predominant (similar to the uncleaned irradiated sample). The C 1s signal increases in intensity and can be fitted using three components: **C**—Se (at ~284.5 eV, peak 1), **C**—C (at ~285.0 eV, peak 2) and **C**—O (at ~286.5 eV, peak 3) while the O 1s signal remains very weak.

4. Discussion

4.1. Peak component analysis

The results for $As_{40}Se_{60}$ films before Ar-ion treatment are summarized in Table 1, where parameters of the components and their contribution to the total core level intensity are given. As can be seen from Table 1 the main component of the Se 3d peak of the non-irradiated sample is As—**Se**—As s.u. (52.8%). Laser irradiation leads to an increase of the intensity of peak 2 and to a small shift of BE from 55.2 eV for the non-irradiated sample to 55.1 eV for the irradiated sample. It can be explained by the formation of additional As—**Se**—Se s.u. accompanied by reduction of the number of As—**Se**—As s.u. Thus, the peak 2 in the Se 3d spectra of the irradiated sample indicates the presence of both As—**Se**—Se and As—**Se**—C s.u. It is important to note the significant contribution of the Se—**Se**—Se s.u. in the Se 3d spectra of both the amorphous and irradiated samples.

The assignment of peak 2 in the Se 3d spectra to **Se**—C bonds is confirmed by the presence of an intense **C**—Se component (peak 1) in the C 1s spectra (see Table 1). Furthermore, the C 1s spectrum contains a graphitic peak at 285.0 eV which becomes the main component in the laser irradiated $As_{40}Se_{60}$ film. Also, the C 1s spectra of both non-irradiated and irradiated films contain **C**—O bonds (peak 3) which correlates with the observed **O**—C bonds in the O 1s spectra.

In contrast to crystalline $As_{40}Se_{60}$ where only As—**Se**—As s.u. (in Se 3d core level spectra) and **As**—3Se (in As 3d core level spectra) s.u. are expected, in our As 3d core level spectra of amorphous non-irradiated films two types of structural units were determined: As—**As**—2Se and **As**—3Se (Table 1). Laser irradiation of the $As_{40}Se_{60}$ film leads to a significant increase in intensity of peak 3 from 58% (non-irradiated sample) to 81% (irradiated sample).

All these facts indicate that the laser irradiation leads to additional Se—Se bond formation with a simultaneous decrease of As—As bond

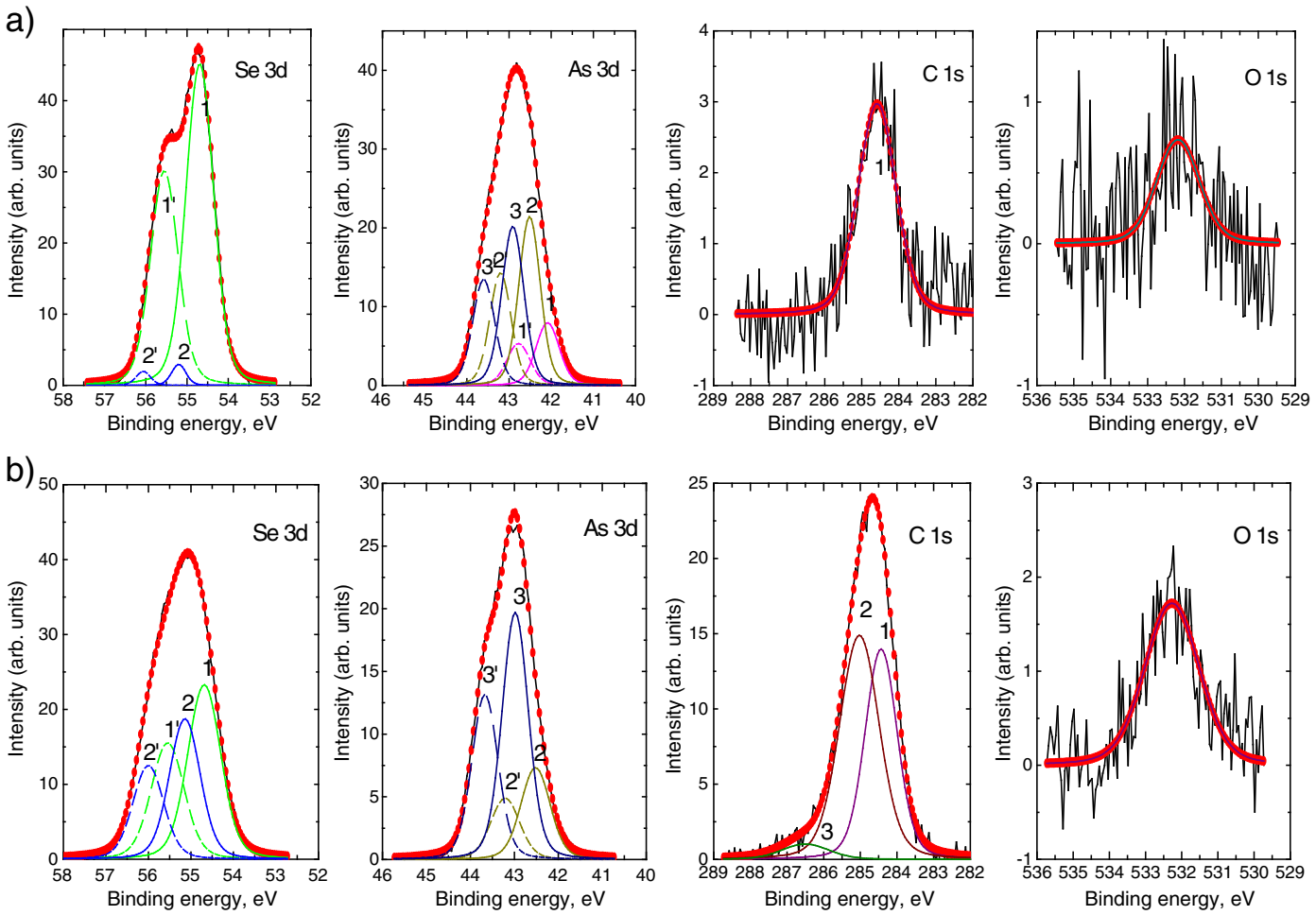

Fig. 2. Se 3d, As 3d, C 1s and O 1s core level spectra of amorphous non-irradiated (a) and irradiated (b) Ar-ion cleaned $As_{40}Se_{60}$ films (black solid line) together with the results of curve fitting (red dots). Se 3d peak components were identified as As—**Se**—As (1), As—**Se**—Se, As—**Se**—C (2); for As 3d – Se—**As**—2As (1), 2Se—**As**—As (2), **As**—3Se (3); for C 1s – **C**—Se (1), **C**—C (2), **C**—O (3); for O 1s – **O**—C. Continuous and dotted lines denote $3d_{5/2}$ and $3d_{3/2}$ peaks, respectively. Photon energies: 450 eV for Se 3d, As 3d and C 1s; 600 eV for O 1s core levels.

concentration. The redistribution of the components' intensities confirms structural changes within the first few surface layers.

To analyze $As_{40}Se_{60}$ layers below the vacuum interface and the laser induced effects occurring in the deeper layers of the film it is very helpful to investigate the SR exited spectra of the samples cleaned by Ar-ion sputtering. Detailed analysis of such data (Fig. 2) was summarized in Table 2. As can be seen from Table 2 a good fit of the Se 3d core level spectra is obtained using two components with the dominant contribution assigned to As—**Se**—As s.u. (97%). The small contribution (3%) of component at BE of 55.2 eV is found to be due to presence of As—**Se**—C s.u. This statement is consistent with the presence of only one **C**—Se component in the C 1s core level spectrum. Also, the absence in the C 1s spectra of the component connected with C—O bonds is confirmed by the negligibly small O 1s signal. It might be connected with the diffusion of carbon into the near surface layers of the sample.

Table 1
Binding energies (BE, ±0.05 eV) and FWHM (±0.01 eV) of individual components determined from curve fitting of Se 3d, As 3d, C 1s and O 1s SRPES spectra of amorphous non-irradiated and irradiated $As_{40}Se_{60}$ films before Ar-ion treatment and their contribution (area, ±4%) to the main ($3d_{5/2}$) peak of each doublet (Se 3d and As 3d are considered).

Peak number	Core level/ component	Non-irradiated sample			Irradiated sample		
		BE	FWHM	Area, %	BE	FWHM	Area, %
	Se 3d:						
Peak 1	As—**Se**—As	54.7	0.85	53	54.7	0.96	37
Peak 2	As—**Se**—Se(C)	55.2	0.58	30	55.1	0.77	43
Peak 3	Se—**Se**—Se	55.6	0.50	17	55.6	0.67	20
	As 3d:						
Peak 2	As—**As**—2Se	42.5	0.79	42	42.5	0.82	19
Peak 3	**As**—3Se	42.9	0.68	58	42.9	0.81	81
	C 1s						
Peak 1	**C**—Se	284.5	0.99	59	284.5	1.10	41
Peak 2	**C**—C	285.0	1.00	33	285.0	1.12	47
Peak 3	**C**—O	286.5	2.08	8	286.5	1.70	12
	O 1s						
Peak 1	**O**—C	532.0	1.51	100	532.0	1.53	100

In contrast to the uncleaned sample the As 3d core level spectra of non-irradiated and Ar-ion cleaned $As_{40}Se_{60}$ film contain an additional As-rich 2As—**As**—Se component. This fact is in a good agreement with As enrichment found for As–Se films in comparison with the corresponding glass source [30,31].

The Se 3d core level spectra of irradiated and Ar-ion cleaned $As_{40}Se_{60}$ film is dominated by the main As—**Se**—As component (57%). Peak 2 become more intensive (from 3% to 43%) and its position shifts to 55.1 eV. As was pointed out before, this indicates the appearance of an As—**Se**—Se s.u. (*i.e.* the formation of additional Se—Se bonds) in the structure of the film under the laser irradiation. It correlates well with the disappearance of the 2As—**As**—Se s.u. in the As 3d core level spectra of the irradiated and Ar-ion cleaned sample and increase of the **As**—3Se s.u. concentration from 41% for the non-irradiated film to 71% for the irradiated sample. The significant increase of C 1s peak intensity (Fig. 2, b) and appearance of the main component (54%)

Table 2
Binding energies (BE, ±0.05 eV) and FWHM (±0.01 eV) of individual components determined from curve fitting of Se 3d, As 3d, C 1s and O 1s SRPES spectra of amorphous non-irradiated and irradiated $As_{40}Se_{60}$ films after Ar-ion treatment and their contribution (area, ±4%) to the main ($3d_{5/2}$) peak of each doublet (Se 3d and As 3d are considered).

Peak number	Core level/ component	Non-irradiated sample			Irradiated sample		
		BE	FWHM	Area, %	BE	FWHM	Area, %
	Se 3d:						
Peak 1	As—**Se**—As	54.7	0.79	97	54.7	0.92	57%
Peak 2	As—**Se**—Se (C)	55.2	0.41	3	55.1	0.86	43%
	As 3d:						
Peak 1	2As—**As**—Se	42.1	0.65	17	–	–	–
Peak 2	As—**As**—2Se	42.5	0.60	42	42.5	0.78	29
Peak 3	**As**—3Se	42.9	0.62	41	42.9	0.70	71
	C 1s						
Peak 1	**C**—Se	284.5	1.21	100	284.5	1.00	41%
Peak 2	**C**—C	–	–	–	285.0	1.20	54%
Peak 3	**C**—O	–	–	–	286.5	1.96	5%
	O 1s						
Peak 1	**O**—C	–	–	–	532.0	1.78	100

characteristic of **C**—C bonds and minor component (4%) originated from **C**—O bonds were detected. The intensity of the latter component correlates well with the small intensity peak at ~532.0 eV characteristic of **O**—C bonds in the O 1s core level spectra. This indicates laser stimulated carbon diffusion into deeper layers of the $As_{40}Se_{60}$ film.

4.2. Structural modifications of $As_{40}Se_{60}$ film after the laser irradiation in air

The analysis of peak intensities of As 3d, Se 3d, C 1s and O 1s spectra of amorphous non-irradiated and irradiated $As_{40}Se_{60}$ film and As to Se ratio before and after Ar-ion sputtering is shown in Table 3. As can be seen, the main component detected in the surface of $As_{40}Se_{60}$ film before Ar-ion treatment is carbon (49%). The laser irradiation leads to a further increase in the concentration of carbon (58%) and a decrease the other components.

The As to Se ratio in this carbon-rich structure is found to be 0.41 for the non-irradiated and 0.40 for the irradiated sample, significantly less than producted. Similar decreasing of As/Se ratio was observed for other compopsitions (As_4Se_4 and As_4Se_3 films) when the as-prepared samples were exposed to air [30,31].

In contrast with the amorphous uncleaned sample the results of measurements performed on Ar-ion sputtered samples, which provide information from deeper layers of the film, show mainly Se (52.8%) and As (43.3%) signals with a small contribution of impurities (C and O signals) (see Table 3). In this case the As/Se ratio increases by a factor 2 in comparison with the uncleaned film. It should be noted here that the As/Se ratio for the cleaned film was calculated at 0.82 which is higher than theoretical one, 0.67. This result can be understood from the analysis of some peculiarities of thermal evaporation process. The arsenic trisulfides (and triselenides) mass-spectrometry studies show the presence of significant amount of As-rich cage like molecules (As_4S_4, As_4S_3) in the vapor in addition to most stable big stoichiometric As_6S_9 molecules [32]. In contrast to bulk As_2S_3 glasses, the structure of amorphous As_2S_3 films prepared by thermal evaporation shows characteristic features of molecular structure of vapor as suggested by our previous Raman study [33]. The less clear evidence of the formation of As-rich As–Se clusters in the structure of As_2Se_3 films is provided by Raman spectroscopy. Therefore, the formation of such molecules (As_4Se_4 and/or As_4Se_3) in As–Se vapor then this can be one of the reasons leading to As enrichment of deposited As–Se film since the lighter Se-dimmers and/or small Se_n-rings ($n<8$) are more effectively removed by vacuum system.

Table 3
Atomic concentrations, As/Se ratio of non-irradiated and irradiated $As_{40}Se_{60}$ film calculated from SRPES data and absolute change of component concentrations.

$As_{40}Se_{60}$ sample		As, %	Se, %	As/Se	C, %	O, %
Before Ar-ion treatment	Non-irradiated	12.7	30.8	0.41	49.0	7.5
	Irradiated	10.1	24.9	0.40	57.7	7.3
Delta (ir.-am.), %:		−2.6	−5.9		+8.7	−0.2
After Ar-ion treatment	Non-irradiated	43.3	52.8	0.82	3.1	0.9
	Irradiated	24.5	46.9	0.52	26.3	2.3
Delta (ir.-am.), %:		−18.8	−5.4	+23.2	+1.4	

The laser irradiation of the sample shows a significant increase of carbon concentration (26.3%) with a simultaneous decrease of the As content (24.5%). The As/Se ratio became 0.52 in comparison with 0.82 calculated for the non-irradiated film.

4.3. Atomic model of induced structural self-organization of the $As_{40}Se_{60}$ nanolayers

Obtained results and their analysis allow us to describe the processes occurring on top surface layer(s) of $As_{40}Se_{60}$ chalcogenide due to air exposure and laser irradiation, and construct an atomistic model.

Our results clearly show a significant decrease of arsenic concentration on the surface of $As_{40}Se_{60}$ film when the sample was exposed to air and/or irradiated. Similar losses of As immediately after exposure to air of an As–Se sample were also reported by other authors [34–36]. Antoine et al. observed that the As/Se ratio decreases immediately after the sample was oxidized (exposed to O_2) and further light illumination leads to only very small changes in the As/Se ratio [37,38]. They pointed out that the reduced amount of arsenic could be due to preferential sublimation of As atoms under ultra high vacuum condition. Some authors relate the change of the As/Se ratio to desorption of relatively more volatile arsenic oxides, i.e. As_2O_3, which is actively formed on the surface during laser irradiation [38]. Such interpretations, however, do not correlate with the interesting observation of the As/Se ratio recovering after thermal treatment of the material [35]. An alternative idea has been proposed by Krishnaswami et al. who pointed out that light induced changes of the surface composition could be due to preferential segregation of selenium from the bulk to the surface [30]. Their suggestion is based on different site defect formation energies for Se and As, resulting in diffusion of atoms with the lowest defect formation energy (Se) to the surface. If the surface composition of a film exposed to air is enriched by Se, then one would expect to observe As-rich layers deeper in the bulk. Our component analysis for the Se 3d spectra shows the presence of a large amount of Se—Se bonds. On the other hand, we have not detected a contribution of oxidized arsenic (As_2O_3) in the experimental As 3d peak for this sample. Such a contribution is expected when an As-rich sample is exposed to air [39]. The changes of the surface composition of the chalcogenide film and its stability in the bulk were supported by our previous studies of Auger spectra of a complex $Ge_{33}As_{12}Se_{55}$ film [40] where losses of As accompanied by the enrichment of Ge and Se in the near surface layers were observed. Therefore, the segregation of Se can mainly be due to evaporation of more volatile arsenic trioxide resulting in drastic losses of As from the surface. The absence of As enriched layers in the bulk allow us to conclude that As_2O_3 volatility is the main feature causing the decreases of arsenic concentration. As a result we observed surface enrichment by Se atoms and formation of additional Se—Se bonds and interface Se—C bonds (due to adsorption from the air). This leads to the formation of a large As gradient concentration from the bulk ($As>40\%$) to the top surface layer ($As\rightarrow 0\%$) of the film.

It is known that diffusion and interdiffusion processes can be induced by light in multiplayer chalcogenide systems [41–43]. The near band gap laser irradiation causes the concentration gradient to be reduced through bond breaking and diffusion of the As atoms from deeper layers to the surface. At the same time, under ambient conditions the arsenic at the surface oxidizes and additional evaporation of arsenic oxides takes place, as seen from the calculated As/Se ratio. As a result,

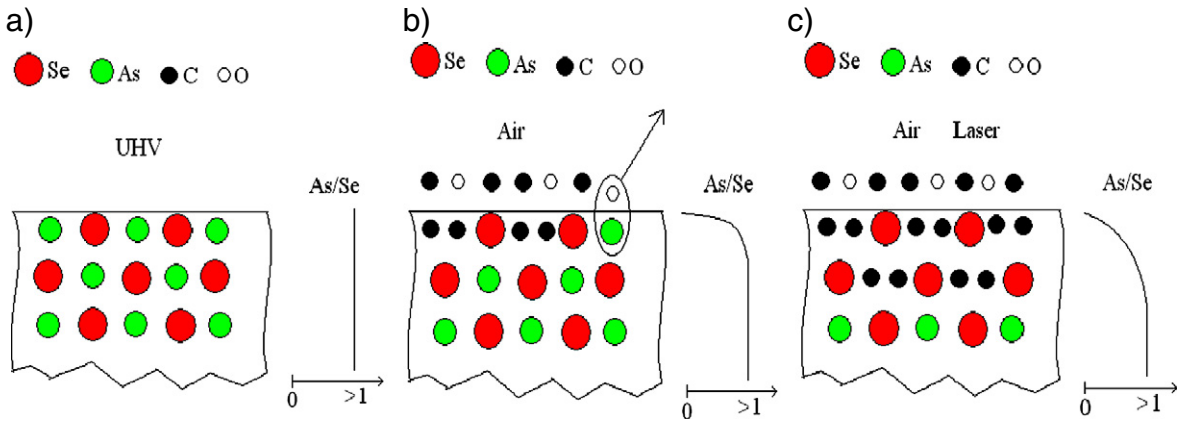

Fig. 3. Atomic model of induced structural changes on the surface of $As_{40}Se_{60}$ nanolayers: a—as deposited film; b—film in air; c—film after laser irradiation in air.

the near surface layers are continuously depleted of arsenic atoms. Simultaneously the carbon partially diffuses into deeper layers. This is clearly seen from the behavior of C 1s peak intensity together with changes of As concentration on the surface and appearance of additional C—Se component in the fitted C 1s spectra (peak 2) of irradiated film (Fig. 2, Table 3).

Additional support of this interpretation is provided by the calculated delta parameters (see Table 3) indicating the differences between atomic concentrations in the non-irradiated and irradiated samples before and after Ar-ion sputtering. The significant decrease of arsenic concentration in irradiated and cleaned sample ($\Delta = -18.8\%$) is accompanied by a significant ($\Delta = +23.2\%$) increase of carbon concentration.

Therefore, under laser irradiation in air the photoinduced structural changes in the bulk already described in detail [36,39] are totally different from the surface processes which cause significant changes of surface stoichiometry and bonding properties. The latter processes are schematically shown in our atomic model of structural changes of the $As_{40}Se_{60}$ nanolayers surface (Fig. 3).

5. Conclusions

The local structural changes of $As_{40}Se_{60}$ nanolayers induced by air and near bandgap laser irradiation have been studied in detail using synchrotron radiation photoelectron spectroscopy. The results, together with spectral analysis of the photoinduced processes, lead to the following conclusions:

(1) Formation of Se—C s.u. on the surface of amorphous $As_{40}Se_{60}$ film exposed to ambient conditions and crucial changes of surface stoichiometry are found to be mainly due to arsenic oxidization and the evaporation of more volatile As_2O_3. This leads to the Se enrichment of the surface layer and formation of a gradient of composition.

(2) Near bandgap laser illumination of the $As_{40}Se_{60}$ thin film stimulates the diffusion process of As atoms from deeper layers to the surface, decreasing the composition gradient. However, subsequent oxidization of arsenic at the surface–air interface and evaporation of As_2O_3 takes place.

(3) Near bandgap laser irradiation leads to significant redistributions of concentrations of As- and Se-centered structural units on the sample surface: the concentration of As—**Se**—Se and **As**—3Se components increases while the **As**-rich Se—**As**—2As and 2Se—**As**—As s.u. in the irradiated sample disappears. Such a transformation implies an increase of the number of As—Se and Se—Se bonds and a simultaneous decrease of the number of As—As bonds in the structure of the irradiated films.

(4) Near bandgap laser irradiation of $As_{40}Se_{60}$ films stimulates diffusion of carbon into the near surface layers, which significantly changes the structural, mechanical and optical properties of sample. Such changes should be considered when using $As_{40}Se_{60}$ films for different applications.

(5) An atomic model of induced structural changes on the surface of $As_{40}Se_{60}$ nanolayers under ambient conditions and laser irradiation in air was proposed.

Acknowledgments

The authors wish to thank Dr. M. Veres (Institute for Solid State Physics and Optics, Wigner Research Center for Physics of the Hungarian Academy of Sciences) for his assistance with Raman monitoring of laser irradiation of the sample. R.H., N.P. and O.K. gratefully acknowledge the support of projects 20100175 and 20105468 from International Center of Theoretical Physics. The Materials Science Beamline is supported by the Ministry of Education of the Czech Republic under Grant No. LC 06058 and by the Czech Grant Agency under contract number AS CR IAA1010143.

References

[1] B.T. Kolomiets, Phys. Status Solidi 7 (359–372) (1964) 713–731.
[2] N.F. Mott, E.A. Davis, Electronic Processes in Non-crystalline Materials, Oxford Univ. Press, London, England, 1971.
[3] A. Felts, Amorphous and Vitreous Inorganic Solids, Mir, Moscow, 1986. (in Russian).
[4] A.V. Kolobov, J. Tominaga, J. Mater. Sci. Mater. Electron. 14 (2003) 677–680.
[5] K. Tanaka, Rev. Solid State Sci. 4 (1990) 641–659.
[6] K. Shimakawa, A. Kolobov, S.R. Elliott, Adv. Phys. 44 (1995) 475–588.
[7] N.P. Eisenberg, M. Manevich, M. Klebanov, S. Shutina, V. Lyubin, Proc. SPIE Int. Soc. Opt. Eng. 2426 (1995) 235–241.
[8] P. Krecmer, A.M. Moulin, R.J. Stephenson, T. Rayment, M.E. Welland, S.R. Elliott, Science 277 (1997) 1799–1802.
[9] V.L. Averyanov, A.V. Kolobov, B.T. Kolomiets, V.M. Lyubin, J. Non-Cryst. Solids 45 (1981) 343–353.
[10] V.M. Lyubin, V.K. Tikhomirov, J. Non-Cryst. Solids 114 (1989) 133–135.
[11] K. Tanaka, K. Ishida, J. Non-Cryst. Solids 227-230 (1998) 673–676.
[12] H. Hamanaka, K. Tanaka, A. Matsuda, S. Iizima, Solid State Commun. 19 (6) (1976) 499–501.
[13] J.S. Berkes, S.W. Ing, W.J. Hillegas, J. Appl. Phys. 42 (1971) 4908–4916.
[14] E. Márquez, J.M. González-Leal, R. Prieto-Alcón, R. Jiménez-Garay, M. Vlcek, J. Phys. D: Appl. Phys. 32 (1999) 3128–3134.
[15] J. Dikova, N. Starbov, K. Starbova, J. Non-Cryst. Solids 167 (1994) 50–58.
[16] R. Holomb, V. Mitsa, P. Johansson, M. Veres, Phys. Status Solidi C 7 (3–4) (2010) 885–888.
[17] O. Kondrat, N. Popovich, R. Holomb, V. Mitsa, O. Petrachenkov, M. Koós, M. Veres, Phys. Status Solidi C 7 (3–4) (2010) 893–896.
[18] Duk-Yong Choi, Steve Madden, Douglas Bulla, Rongping Wang, Andrei Rode, Barry Luther-Davies, J. Appl. Phys. 107 (2010) 053106-6.
[19] H. Valdes, M. Sanches-Polo, C.A. Zador, Lat. Am. Appl. Res. 33 (2003) 219–223.
[20] D. Briggs, M.P. Seah, 2nd ed., Practical Surface Analysis, vol. 1, John Wiley & Sons, New York, NY, USA, 1993.
[21] C.D. Wanger, W.M. Riggs, L.E. Davis, J.F. Moulder, G.E. Muilenberg, Handbook of X-ray Photoelectron Spectroscopy, Perkin-Elmer Corp., Physical Electronics Division, Eden Prairie, Minnesota, USA, 1979.
[22] J.J. Yeh, Atomic Calculation of Photoionization Cross-Sections and Asymmetry Parameters, Gordon and Breach Science Publishers, Langhorne, PE, USA, 1993.

[23] J.J. Yeh, I. Lindau, At. Data Nucl. Data Tables 32 (1985) 1–155.
[24] P.R. Sarode, K.J. Rao, M.S. Hegd, C.N.R. Rao, J. Phys. C 12 (1979) 4119–4128.
[25] T. Ueno, A. Odajima, Jpn. J. Appl. Phys. 20 (1981) L501–L504.
[26] T. Ueno, Jpn. J. Appl. Phys. 22 (1983) 1469–1473.
[27] M.K. Bahl, R.O. Woodall, R.L. Watson, K.J. Irgolic, J. Chem. Phys. 64 (1976) 1210–1226.
[28] P.V. Galiy, A.V. Musyanovych, Funct. Mater. 12 (3) (2005) 467–475.
[29] N. Martensson, A. Nilsson, J. Electron Spectrosc. Relat. Phenom. 52 (1990) 1–46.
[30] S. Krishnaswami, H. Jain, A.C. Miller, J. Optoelectron. Adv. Mater. 3 (3) (2001) 695–702.
[31] K. Antoine, H. Jain, J. Li, D.A. Drabolt, M. Vlček, A.C. Miller, J. Non-Cryst. Solids 349 (2004) 162–167.
[32] P. Martin, Solid State Commun. 47 (2) (1983) 111–114.
[33] R. Holomb, V. Mitsa, O. Petrachenkov, M. Veres, A. Stronski, M. Vlček, Phys. Status Solidi C 8 (2011) 2705–2708.
[34] A.V. Kolobov, Y.P. Kostikov, S.S. Lantratova, V.M. Lyubin, Sov. Phys. Solid State 33 (1991) 444–447.
[35] T. Kitahara, T. Arai, Jpn. J. Appl. Phys. 18 (1979) 1635–1636.
[36] H. Jain, S. Krishnaswami, A.C. Miller, P. Krecmer, S.R. Elliott, M. Vlcek, J. Non-Cryst. Solids 274 (2000) 115–123.
[37] K. Antoine, J. Li, D.A. Drabold, H. Jain, M. Vlchek, A.C. Miller, J. Non-Cryst. Solids 326&327 (2003) 248–256.
[38] K. Antoine, H. Jain, M. Vlchek, S.D. Senanayake, D.A. Drabold, Phys. Rev. B 79 (2009) 054204–054207.
[39] M. Kalyva, A. Siokou, S.N. Yannopoulos, T. Wagner, J. Orava, M. Frumar, J. Non-Cryst. Solids 355 (2009) 1844–1848.
[40] Yu.Yu. Babinets, Yu.B. Gvardionov, L.G. Kesler, V.M. Mitsa, Quantum electron. 38 (1990) 94–96 (in Russian).
[41] K.S. Sangunni, J. Indian Inst. Sci. 91 (2) (2011) 295–302.
[42] K.V. Adarsh, Ramakanta Naik, K.S. Sangunni, S. Kokenyesi, H. Jain, Alfred C. Miller, J. Appl. Phys. 104 (2008) (053501-053501-7).
[43] V. Takats, A.C. Miller, H. Jain, A. Kovalskiy, S. Kokenyesi, Thin Solid Films 519 (10) (2011) 3437–3442.